Modularized Bilinear Koopman Operator for Modeling and Predicting Transients of Microgrids

Xinyuan Jiang, *Graduate Student Member, IEEE,* Yan Li, *Senior Member, IEEE,* and Daning Huang

***Abstract*— Modularized Koopman bilinear form (M-KBF) is presented to model and predict the transient dynamics of microgrids in the presence of disturbances. As a scalable data-driven approach, M-KBF divides the identification and prediction of the high-dimensional nonlinear system into the individual study of subsystems, and thus, alleviates the difficulty of intensively handling high volume data and overcomes the curse of dimensionality. For each subsystem, Koopman bilinear form is established to efficiently identify its model by identifying isotypic eigenfunctions via the Extended Dynamic Mode Decomposition (EDMD) method with an eigenvalue-based order truncation. Extensive tests show that M-KBF can provide accurate transient dynamics prediction for the nonlinear microgrids and verify the plug-and-play modeling and prediction function, which offers a potent tool for identifying high-dimensional systems with reconfiguration feature. The modularity feature of M-KBF enables the provision of fast and precise prediction for the power grid operation and control, paving the way towards online applications.**

***Index Terms*— Modularized Koopman bilinear form (M-KBF), data-driven modeling, Koopman operator, extended dynamic mode decomposition (EDMD), transient dynamics prediction, microgrids, distributed energy resources (DERs).**

I. Introduction

DISTRIBUTED energy resources (DERs), such as photovoltaic (PV) and wind power, are seen as important solutions to modernizing the power system. There have been growing research interests on the application of microgrids for the integration of DERs, which differs from traditional power systems in that the microgrid systems often operate under more severe transient conditions due to the unpredictable nature of the DERs and the larger instantaneous load and generation imbalance compared to the system capacity. Thus, it is of utmost importance to develop generic data-driven modeling and prediction algorithms to assimilate the nonlinear dynamics exhibited during normal microgrid operations, which is closely related to the study of system identification.

Although several nonlinear system identification methods for power systems have been proposed over the past decade, the most widely recognized methods for monitoring the state of power systems are linear methods. Existing linear techniques include model-based linear system identification methods such as Prony's method [1], [2], minimal realization algorithm [3], eigenvalue realization algorithm (ERA) [4], matrix pencil method [5], Hankel total least squares (HTLS) [6], and subspace identification [7]. There are also frequency domain methods such as Yule-Walker [8] and frequency domain decomposition [9] as well as non-parametric frequency analysis methods such as Welch periodgram [10]. Linear methods are useful for assessing system stability by analyzing the changes in the dominant eigenvalues of the system and have been one of the most important methods in studying nonlinear systems due to the abundance of techniques in dealing with linear systems.

Fundamentally, linear system identification methods try to fit the system responses with a linear combination of complex exponential functions, which are good approximations when a single operating point is concerned. However, a typical microgrid system can have highly nonlinear responses spanning a wide range of operating points that cannot be assimilated with complex exponential functions. Therefore, the information obtained from linear methods is lacking to support the operation of a microgrid.

For nonlinear system identification, many existing methods are applicable to the specific types of system and require prior knowledge along with the input and output data of the system. A typical example involves expanding the unknown part of a gray box model into infinite series such as Taylor series [11] and Volterra series [12], and fitting the parameters using linear regression or some nonlinear optimization method. More recently, methods such as sparse identification of nonlinear dynamics (SINDy) [13], neural networks [14], particle filters [15], and expectation-maximization algorithm (EM) [16] aim at identifying general nonlinear systems. However, due to the intractable types of nonlinearities, the ability to obtain a globally optimal solution may vary.

As an emerging class of data-driven modeling methods, Koopman operator has gained significant attention with research in machine learning and control [17]–[20]. The Koopman theory states that dynamical systems in general can be linearized in the function space using the eigenfunctions associated with the infinite-dimensional Koopman operator. This is different from traditional nonlinear identification problems because the focus is shifted from recovering nonlinear equations to finding linearly evolving eigenfunctions in the infinite-dimensional space of observable functions. The advantage of Koopman operator-based methods is that in the coordinates of Koopman eigenfunctions, the equivalent linear dynamics is amenable to linear control [21]–[23], while the difficulty is to numerically approximate those eigenfunctions without general analytical forms to compare against.

This work is supported by National Science Foundation under the award DMS-2229435 and Office of Naval Research under the award N00014-22-1-2504.

X. Jiang and Y. Li are with the Department of Electrical Engineering, The Pennsylvania State University, University Park, PA 16802, USA (e-mail: yql5925@psu.edu).

D. Huang is with the Department of Aerospace Engineering, The Pennsylvania State University, University Park, PA 16802, USA (e-mail: daning@psu.edu).

Based on the linear evolution of Koopman eigenfunctions, the methods for linear system identification are modified through the so-called lifting technique to identify or approximate linearly evolving eigenfunctions within an extensive set of function basis, examples such as generalized Laplace analysis (GLA) [24], extended dynamic mode decomposition (EDMD) [25], kernel EDMD [26], and extended subspace identification [27]. EDMD is by far the most studied with convergence properties characterized in [28]. Various other types of methods [29], [30] exploit the connection between the linearization spectrum and the Koopman spectrum to obtain eigenfunctions on a static basin of attraction.

Data-driven Koopman operator methods have been extensively applied to power system coherence identification [31], Koopman model predictive control [32], [33], and LQR secondary microgrid control with stability guarantee [34], [35]. However, existing methods suffer from two limitations. First, due to the fast response of inverter-based DERs and the extended range of steady-state operating points at the distribution level, microgrids generally exhibit complex nonlinear dynamics that cannot be identified through the direct reduction of coherency of different types of DERs [36]. A data-driven modeling method applied to the microgrid as a whole thus would involve finding eigenfunctions on a much higher-dimensional state space, leading to inefficiency in training data collection and in singular value decomposition for EDMD. Second, most existing Koopman identification or control methods extend poorly to situations where the system receives multiple input disturbances [37], while a data-driven model for microgrid dynamics needs to include the disturbances to DER power or load power, thus limiting the number of control and power components in the network.

To address the above limitations, a distributed data-driven Koopman method is proposed in this paper called modularized Koopman bilinear form (M-KBF) for the modeling and prediction of microgrid nonlinear dynamics. Similar to existing modular modeling methods that decompose the system according to the interaction between modules through the input and output voltage and current [38], the task of Koopman modeling the high-dimensional microgrid dynamics is reduced to problems of modeling each module (DER subsystem) with bilinear inputs [39], [40]. In this configuration, the interaction between the modules serves as the excitation for the identification of the dynamics of each module, instead of relying on external inputs that can interrupt the operation of the microgrid. At the same time, the large number of input disturbances to the system assigned to each module can be clearly distinguished in their effect towards the whole system.

The contributions of this paper are:

- A distributed data-driven modeling method (M-KBF) that combines the bilinear Koopman operator modules in network to study the nonlinear dynamics of microgrids with reduced data-sharing
- An algorithm for predicting microgrid dynamics with the data-driven M-KBF model which stands out for its flexibility and scalability: It is capable of predicting the dynamics across various microgrid topologies, distinct from the training data, by only necessitating the retraining of new bus dynamics because of the explicit network structure of M-KBF model.
- An isotypic observable dictionary that preserves the angle symmetry of the dynamics in the Koopman bilinear model for accurately predicting the complex nonlinear interactions that constitute the microgrid dynamics.

The remainder of this paper is organized as follows. Section II establishes the modularized Koopman bilinear form. Section III introduces the determination of eigenfunctions through the EDMD method with order truncation. Section IV presents the prediction of transient dynamics based on M-KBF. In Section V, tests on a microgrid system verify the effectiveness and efficiency of the presented method in modeling and predicting transients. Conclusions are drawn in Section VI.

II. Modularized Koopman Bilinear Form

A microgrid consists of a local connection of DERs and loads by an electrical network of electrical lines. Each connection point between the electrical network to a DER or load is a bus with its instantaneous bus voltage and bus current. Each DER subsystem with the renewable source interfaced by the power electronics control apparatus is connected to the electrical network through its bus voltage and bus current. The objective of identification through M-KBF is to build individual KBF models for each DER subsystem up to the bus connection with the network as in Fig. 1, while the electrical network being linear algebraic equations can be calculated in advance through the known or identified line impedance data.

A. Overview of M-KBF Model and the Network Equations

The data-driven modeling of the microgrid system by M-KBF begins with modeling the electrical network as a hybrid parameter matrix [41]. The hybrid parameter matrix, which is derived from the power network's nodal admittance matrix, maps from a set of bus voltages and currents to bus currents and voltages of the same buses. The input and output equations of the network model is written as

$$\mathbf{y}^{\text{net}} = \mathbf{H}\mathbf{u}^{\text{net}} \tag{1}$$

with

$$\mathbf{y}^{\text{net}} = \begin{bmatrix} \underline{I}_1 \\ \underline{V}_2 \end{bmatrix}, \mathbf{u}^{\text{net}} = \begin{bmatrix} \underline{V}_1 \\ \underline{I}_2 \end{bmatrix}, \tag{2}$$

where subscript 1 denotes the set of grid-forming (GFM) buses, and subscript 2 denotes the set of grid-following (GFL) and/or load buses. Then, the internal bus dynamics of either DERs or power loads from $\underline{I}_1$ to $\underline{V}_1$ (from $\underline{V}_2$ to $\underline{I}_2$) are fitted through KBF models, with the bus voltage and current as the interaction between the network model (1) and the internal bus dyanmics. Since each bus can have different functionalities in balancing power injection and maintaining overall stability, namely GFM or GFL [42], [43], the input to the internal bus dynamics is either the bus current or the bus voltage. The condition and formula for the hybrid parameter matrix from the nodal admittance matrix is provided in the Appendix.

The DER system shown in Fig. 1 interacts with the network through the bus voltage V_C and current I_N. The input of the

DER internal dynamics depends on whether the control is GFM or GFL. GFM control regulate the voltage and maintains overall stability under constant perturbations in power supply and demand, so the input of the GFM dynamics is the bus current. GFL control regulate their individual power output with no stability functionality to the overall system, thus the input of the GFL dynamics is the bus voltage.[1] Additionally, GFL DER systems can receive power reference inputs as their target power outputs.

Denote the set of buses of the microgrid as $\mathcal{N}$ and the subsets of GFM and GFL buses as respectively $\mathcal{N}_1$ and $\mathcal{N}_2$ such that $\mathcal{N}_1 \cup \mathcal{N}_2 = \mathcal{N}$, $\mathcal{N}_1 \cap \mathcal{N}_2 = \emptyset$. The two type of DER bus dynamics can be written in general as the following control-affine systems

$$\text{GFM: } \dot{\mathbf{x}}_p = \mathbf{f}_p(\mathbf{x}_p) + \mathbf{G}_p(\mathbf{x}_p) I_{1,p}^{\text{gen}},\ p \in \mathcal{N}_1 \tag{3a}$$

$$\text{GFL: } \dot{\mathbf{x}}_p = \mathbf{f}_p(\mathbf{x}_p) + \mathbf{G}_p(\mathbf{x}_p) \left[V_{2,p}^{\text{gen}},\ S_p^{\text{ref}}\right]^{\mathsf{T}},\ p \in \mathcal{N}_2 \tag{3b}$$

where $\mathbf{x}_p \in \mathbb{C}^{n_p}$ is the state vector of the internal dynamics, $I_{1,p}^{\text{gen}}$, $V_{2,p}^{\text{gen}}$ are the DER generator current and voltage of bus p, and S_p^{ref} is the complex power reference input for the GFL control.

The power loads can be modeled as GFL buses with negative power reference input. In this paper, the power loads are modeled by their instantaneous complex power. In general, we can define a constant power load at every bus $k \in \mathcal{N}$ by allowing zero load power. Denote the load power and load current respectively as

$$\underline{S}^{\text{ld}} = \begin{bmatrix} \underline{S}_1^{\text{ld}} \\ \underline{S}_2^{\text{ld}} \end{bmatrix},\ \underline{I}^{\text{ld}} = \begin{bmatrix} \underline{I}_1^{\text{ld}} \\ \underline{I}_2^{\text{ld}} \end{bmatrix}. \tag{4}$$

Using the definition of complex power, we can combine the network model (1) with the load constraints (4) to get

$$\underline{S}^{\text{ld}} = \text{diag}\Big(\begin{bmatrix} \underline{V}_1^{\text{gen}} \\ \mathbf{H}_{21}\underline{V}_1^{\text{gen}} + \mathbf{H}_{22}\big(\underline{I}_2^{\text{gen}} + \underline{I}_2^{\text{ld}}\big) \end{bmatrix} \Big) \text{conj}\big(\underline{I}^{\text{ld}}\big), \tag{5}$$

where $\mathbf{H}_{21}$ and $\mathbf{H}_{22}$ are the appropriate submatrices of $\mathbf{H}$. The constraint (5) is used for solving the load current $\underline{I}^{\text{ld}}$ given the outputs of the DER dynamics $\underline{V}_1^{\text{gen}}$ and $\underline{I}_2^{\text{gen}}$ at each time step. We refer to (5) as the hybrid power flow equations because from its solution for $\underline{I}^{ld}$ we obtain the vector of inputs to the DER dynamics as

$$\begin{bmatrix} \underline{I}_1^{\text{gen}} \\ \underline{V}_2^{\text{gen}} \end{bmatrix} = \mathbf{H} \begin{bmatrix} \underline{V}_1^{\text{gen}} \\ \underline{I}_2^{\text{gen}} + \underline{I}_2^{\text{ld}} \end{bmatrix} - \begin{bmatrix} \underline{I}_1^{ld} \\ \underline{0} \end{bmatrix}. \tag{6}$$

B. KBF Model for the DERs

In this subsection, we introduce the Koopman bilinear form (KBF) of (3) for GFM and GFL DERs in the function space, while the data-driven procedure is discussed in the next section. The discussion of KBF in this section is based on

[1]From a mathematics perspective, either bus current or voltage can be chosen as the input for either GFM or GFL bus dynamics. However, the causal relation between the bus voltage and current is different for GFM and GFL controls. The specific inputs for GFM and GFL bus dynamics is found to be imperative to the success of the data-driven modeling in our tests.

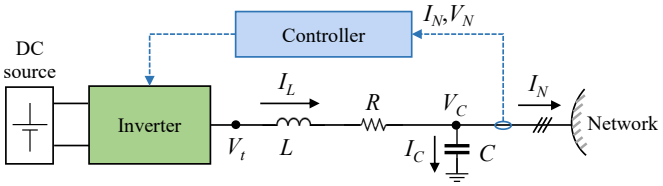

Fig. 1. Schematics of the DER system

complex state space and complex valued functions, which is suited to the study of power networks expressed in terms of complex voltage and current phasors. We begin by considering the general control-affine system of the following form before specializing to the case of DER dynamics (3):

$$\dot{\mathbf{x}} = \mathbf{f}(\mathbf{x}) + \sum_{i=1}^{m} \mathbf{g}_i(\mathbf{x}) u_i \tag{7}$$

The KBF of (7) is introduced in the following three aspects.

1) Observable Function: An observable function $\varphi : \mathbb{R}^n \to \mathbb{C}$ is a complex-valued function of the state vector $\mathbf{x}$. Let $\mathcal{F}$ be a suitable function space, e.g., $\mathcal{C}^1$, so that $\varphi \in \mathcal{F}$. Let $\mathbf{\Phi}_{\mathbf{u}}(t, \mathbf{x}_0)$ be the flow map of the system (7) at time $t > 0$ starting from an initial condition $\mathbf{x}_0$ with input $\mathbf{u}$. The time-varying observable $\psi(t, \mathbf{x}) \triangleq \varphi(\mathbf{x})\big|_{\mathbf{x}=\mathbf{\Phi}_{\mathbf{u}}(t,\mathbf{x}_0)}$ of the system (7) is the solution of the following partial differential equation, which is the starting point for bilinearization.

$$\begin{aligned} \frac{\partial \psi}{\partial t} &= L_{\mathbf{f}}\psi + \sum_{i=1}^{m} u_i L_{\mathbf{g}_i}\psi, \\ \psi(0, \mathbf{x}) &= \varphi(\mathbf{x}), \end{aligned} \tag{8}$$

where $L_{\mathbf{f}} \triangleq \mathbf{f} \cdot \nabla$, $L_{\mathbf{g}_i} \triangleq \mathbf{g}_i \cdot \nabla$, $i = 1, \ldots, m$ are the Lie derivatives [44] with respect to the drift and control vector fields $\mathbf{f}(\mathbf{x})$ and $\mathbf{g}_i(\mathbf{x})$, which are linear operators on $\mathcal{C}^1$.

2) Koopman Operator: The Koopman operator is defined for the unactuated part of the system (7)

$$\dot{\mathbf{x}} = \mathbf{f}(\mathbf{x}). \tag{9}$$

Assume $\mathbf{\Phi}(t, \mathbf{x}_0)$ is the flow map of (9) for time $t > 0$, the continuous-time Koopman operator is defined as $\mathcal{K}^t : \mathcal{F} \to \mathcal{F}$ such that,

$$(\mathcal{K}^t \varphi)(\cdot) = \varphi \circ \mathbf{\Phi}(t, \cdot), \tag{10}$$

where $\circ$ represents function composition. Based on (10), we can see that the Koopman operator is linear, namely,

$$\begin{aligned} \mathcal{K}^t(\alpha_1\varphi_1 + \alpha_2\varphi_2) &= \alpha_1\varphi_1 \circ \mathbf{\Phi}(t, \cdot) + \alpha_2\varphi_2 \circ \mathbf{\Phi}(t, \cdot) \\ &= \alpha_1 \mathcal{K}^t\varphi_1 + \alpha_2 \mathcal{K}^t\varphi_2. \end{aligned} \tag{11}$$

Therefore, the Koopman operator can be characterized by its eigenvalues and eigenfunctions,

$$\mathcal{K}^t \phi = e^{t\lambda}\phi, \tag{12}$$

where $\lambda \in \mathbb{C}$ is the Koopman eigenvalue and $\phi \in \mathcal{F}$ is the corresponding eigenfunction.

From the definition of Lie derivatives, the infinitesimal generator of the Koopman operator is equal to the Lie derivative of the drift vector field, i.e., $L_{\mathbf{f}} = \lim_{t \to 0} \frac{\mathcal{K}^t - \mathcal{I}}{t}$, where $\mathcal{I}$ is the identity operator, so $L_{\mathbf{f}}$ is also referred to as the Koopman

generator. The eigenvalue and eigenfunction relation in (12) can also be expressed in terms of the Lie derivative,

$$L_{\mathbf{f}}\phi = \lambda\phi. \tag{13}$$

From (13) and the definition of $L_{\mathbf{f}}$, for any two eigenpairs (λ_1, ϕ_1) and (λ_2, ϕ_2), we have

$$L_{\mathbf{f}}(\phi_1 \cdot \phi_2) = (\lambda_1 + \lambda_2)(\phi_1 \cdot \phi_2). \tag{14}$$

Thus, there exist infinitely many eigenfunctions and eigenvalues for the Koopman operator.

In the same way, we can define Koopman operator for each input-linear part $\dot{\mathbf{x}} = u_i\mathbf{g}_i(\mathbf{x})$ assuming that u_i is constant in time. Due to the mixing of the dynamics in the control-affine system, the overall Koopman operator is no longer affine in the input $\mathbf{u}$ (compare with the Koopman generator in (8)).

3) Bilinearization: The goal of bilinearization of (7) is to choose a set of observable functions,

$$T(\mathbf{x}) = \begin{bmatrix}\varphi_1(\mathbf{x}) & \varphi_2(\mathbf{x}) & \dots & \varphi_M(\mathbf{x})\end{bmatrix}^{\mathsf{T}}, \tag{15}$$

such that their evolution over time is that of a bilinear system (16), which mirrors (8) with the observable function basis $\mathbf{z} = T(\mathbf{x})$.

$$\dot{\mathbf{z}} = \mathbf{A}\mathbf{z} + \sum_{i=1}^{m} u_i\mathbf{B}_i\mathbf{z}, \quad \mathbf{z}(0) = T(\mathbf{x}_0), \tag{16}$$

where $\mathbf{A}$ and $\mathbf{B}_i$ will be determined in Section III. The condition for bilinearizability into the form (16) using, as the observable functions, the infinite number of eigenfunctions of $L_{\mathbf{f}}$, is provided by Theorem 1 from [40]. And furthermore, bilinearizability condition with finite eigenfunction embeddings is provided in the following theorem for completeness.

Theorem 1: [[40, Theorem 2]] If a set of Koopman eigenfunctions $\phi_1, \phi_2, \dots, \phi_M$ of the unactuated system forms an invariant subspace for every $L_{\mathbf{g}_i}$, $i = 1, \dots, m$, then the system (7) is bilinearizable with the M-dimensional embedding $\phi_1, \phi_2, \dots, \phi_M$.

4) Isotypic Embedding for DER Dynamics: An important property of the DER system (3) which should be preserved in the KBF model is that the system (3) remains invariant as the angle reference is changed. Such dynamical systems are called symmetric, where one trajectory of the system always implies the existence of a symmetry transformed trajectory. Because the KBF models for DER dynamics to be separately identified need to predict the collective behavior of the microgrid including the interaction between DER systems, it is necessary that the KBF models preserve this symmetry to avoid erroneous dynamics in the prediction. One such way is to non-dimensionalize the state vector of the system to obtain a KBF model in isotypic function space that is independent to the symmetry of the underlying system [45] We illustrate how to obtain isotypic embedding with the examples of Vf control.

Voltage frequency (Vf) control is an example of GFM control (3a). The state vector and the input can be expressed as

$$\mathbf{x} = \begin{bmatrix}\mathbf{x}_1, \theta, I_L, V_C\end{bmatrix}^{\mathsf{T}}, \mathbf{u} = I_N, \tag{17}$$

where $\mathbf{x}_1 \in \mathbb{R}^5$ is the controller state vector in the internal reference frame, $\theta \in \mathbb{R}$ is the angle of the internal reference frame relative to the external reference frame, and $I_L, V_C, I_N \in \mathbb{C}$ are the RLC filter currents and voltages in the external reference frame. The internal reference frame is provided by the controller to transform the three-phase signals into phasors, while the external reference frame is shared between the DER system and the network. The symmetry of the system involves the angles of θ, I_L, V_C and I_N. Notice in this case, that we can identify another symmetry involving the scaling of $\alpha e^{j\theta}$, I_L, V_C and I_N, where $\alpha = 1$ without the scaling of the trajectory. Thus, we define the non-dimensional state vector and input as

$$\mathbf{x}' = \begin{bmatrix}\mathbf{x}_1, \dfrac{e^{j\theta}}{V_C}, \dfrac{I_L}{V_C}\end{bmatrix}^{\mathsf{T}}, \mathbf{u}' = \frac{I_N}{V_C}, \tag{18}$$

and the isotypic observable functions are written as

$$\varphi^q(\mathbf{x}) = \overline{\varphi}^q\left(\mathbf{x}_1, \frac{e^{j\theta}}{V_C}, \frac{I_L}{V_C}\right) V_C^{-q}, \tag{19}$$

where $q \in \mathbb{Z}$ is the isotypic index [45]. The isotypic observable function with isotypic index q has the property that it has a single frequency $(q/2\pi)$ with respect to symmetry transformation, i.e., simultaneous shifting of the angles of $e^{j\theta}$, I_L, V_C, and it can be seen in (16) that this embedding guarantees the symmetry of the KBF model without even considering the accuracy of the approximated eigenfunctions. Using the invariance of the Koopman operator in isotypic subspaces [45] and the group property of Koopman operator (14), all possible groups of eigenfunctions can be found in one isotypic subspace. Thus, in the training of the KBF model, it is sufficient to choose the observable dictionary to have the same isotypic index $q \neq 0$; $q = 0$ is a degenerate case where the global angle dynamics is eliminated from the KBF model.

Constant power (PQ) is an example of GFL control (3b) with the state vector and input

$$\mathbf{x} = \begin{bmatrix}\mathbf{x}_1, \theta, I_L\end{bmatrix}^{\mathsf{T}}, \mathbf{u} = \begin{bmatrix}V_C, S^{\mathrm{ref}}\end{bmatrix}^{\mathsf{T}}. \tag{20}$$

The isotypic observable function is found by separating the angle symmetry as

$$\varphi^q(\mathbf{x}) = \overline{\varphi}^q\left(\mathbf{x}_1, \frac{I_L}{e^{j\theta}}\right) e^{-jq\theta} \tag{21}$$

with the non-dimensional state and input

$$\mathbf{x}' = \begin{bmatrix}\mathbf{x}_1, \dfrac{I_L}{e^{j\theta}}\end{bmatrix}^{\mathsf{T}}, \mathbf{u}' = \begin{bmatrix}\dfrac{V_C}{e^{j\theta}}, \dfrac{S^{\mathrm{ref}}e^{j\theta}}{V_C}\end{bmatrix}^{\mathsf{T}}, \tag{22}$$

where, as in the case of Vf control, we can choose a single isotypic space with $q \neq 0$ as the embedding space for the KBF model. In the remaining part of this paper, we choose the isotypic index $q = -1$ for both Vf and PQ systems without loss in expressiveness.

In the next section, the data-driven method for approximating finite-dimensional Koopman invariant subspaces is developed for DER subsystems based on the EDMD algorithm.

III. Data-Driven Identification of KBF

The data-driven identification of the KBF equivalent model (16) of the DER subsystem is performed through a least-squares formulation using a predetermined set of observable functions. The eigenfunction embeddings and the KBF system are identified simultaneously from the state and input measurements of the DER subsystems.

The general rule for selecting a dictionary of observable functions is that these functions should span a rich subspace so that a certain set of eigenfunctions can be approximated by their projections onto this subspace. There are several choices of observable functions [46], including monomials, radial basis functions, Hermite and Chebyshev polynomials. In this paper, we choose the real monomial functions for building the first part $\bar{\varphi}^1(\mathbf{x})$ of the isotypic observable function, (19) or (21), to cover the function space of polynomials up to a certain order. Thus we have

$$T(\mathbf{x}) = \left[\bar{\varphi}_1(\mathbf{x}')\ \bar{\varphi}_2(\mathbf{x}')\ \dots\ \bar{\varphi}_M(\mathbf{x}')\right]^{\mathsf{T}} V_C \tag{23}$$

in the case of GFM DER, or

$$T(\mathbf{x}) = \left[\bar{\varphi}_1(\mathbf{x}')\ \bar{\varphi}_2(\mathbf{x}')\ \dots\ \bar{\varphi}_M(\mathbf{x}')\right]^{\mathsf{T}} e^{j\theta} \tag{24}$$

in the case of GFL DER. The real monomials $\bar{\varphi}_i(\mathbf{x}')$ are functions of the real and imaginary parts of its arguments and are important for implementing the error correction step in prediction. The monomials, in particular, include the (zeroth-order) constant function and the first-order monomials so that the outputs of the GFM and GFL systems can be found in the dictionary as

$$\text{GFM:}\ \ \mathbf{y} = 1 \cdot V_C, \tag{25a}$$

$$\text{GFL:}\ \ \mathbf{y} = \left[\mathrm{Re}\left(\frac{I_L}{e^{j\theta}}\right) + j\mathrm{Im}\left(\frac{I_L}{e^{j\theta}}\right)\right] \cdot e^{j\theta}. \tag{25b}$$

The data-driven EDMD algorithm for fitting the KBF model is discussed next.

A. Approximated Eigenfunctions

Given the conditions in Theorem 1, the original system (7) can be identified by the KBF model (16) in the coordinates of a finite invariant set of eigenfunctions of $L_{\mathbf{f}}$. One option to approximate such invariant sets of eigenfunctions is by applying EDMD on the sampled trajectories of the system with zero inputs [40]. However, as the inputs to DER subsystems include node current or voltage that cannot be held constant during system transients, it is not feasible to independently identify the eigenfunctions using EDMD. Instead, the invariant eigenfunction embeddings and the bilinear system can be identified together using a predetermined dictionary of observable functions.

The requirement on the observable functions is that their span covers an invariant eigenspace of $L_{\mathbf{f}}$ with respect to (8), which is defined in Theorem 1. Then, given a finite KBF system (16) and the observable functions $T(\mathbf{x})$, for each left eigenvector $\mathbf{w}_i$ and eigenvalue λ_i of $\mathbf{A}$, $\phi(\mathbf{x}) = \mathbf{w}_i^{\mathsf{H}} T(\mathbf{x})$ can be shown to be an eigenfunction of $L_{\mathbf{f}}$ with eigenvalue λ_i [37]. Assuming that $\mathbf{A}$ is diagonalizable, denote the left eigenvector matrix $\mathbf{W}$ and eigenvalue matrix $\mathbf{D}$ of $\mathbf{A}$ such that $\mathbf{W}^{\mathsf{H}}\mathbf{A} = \mathbf{D}\mathbf{W}^{\mathsf{H}}$. Then the approximated eigenfunction embeddings $\widetilde{\mathbf{z}} = \mathbf{W}^{\mathsf{H}}\mathbf{z} = \mathbf{W}^{\mathsf{H}} T(\mathbf{x})$ is a linear transformation of the predetermined observable function embeddings, which gives us the following KBF system with the eigenfunction embedded state,

$$\dot{\widetilde{\mathbf{z}}} = \mathbf{D}\widetilde{\mathbf{z}} + \sum_{i=1}^{m} u_i \widetilde{\mathbf{B}}_i \widetilde{\mathbf{z}}, \quad \widetilde{\mathbf{z}}(0) = \mathbf{W}^{\mathsf{H}} T(\mathbf{x}_0), \tag{26}$$

where $\widetilde{\mathbf{B}}_i = \mathbf{W}^{\mathsf{H}}\mathbf{B}_i(\mathbf{W}^{\mathsf{H}})^{-1}$.

B. Discretization of KBF for Identification

Since the measurement data are discrete-time data, the continuous-time KBF system (16) needs to be discretized to provide the discrete-time template for identification. Again, we assume that the span of the observable functions $T(\mathbf{x})$ covers an invariant eigenspace of $L_{\mathbf{f}}$. Assume the sampling period is Δt and that the inputs $u_i(t)$ are constant within each time step (zero-order hold). The KBF system is linear time-invariant with the solution (27) within each time step.

$$\mathbf{z}(t+\Delta t) = \exp\left[\left(\mathbf{A} + \sum_{i=1}^{m} u_i(t+\Delta t)\mathbf{B}_i\right)\Delta t\right]\mathbf{z}(t) \tag{27}$$

Then, by expanding (27) into Taylor series and taking the first order approximation on Δt, we can get the discretized KBF model in explicit (28a) and implicit (28b) forms:

$$\mathbf{z}_{k+1} = \mathbf{A}^d\,\mathbf{z}_k + \sum_{i=1}^{m} u_{i,k+1}\mathbf{B}_i^d\,\mathbf{z}_k + \mathcal{O}(\Delta t^2), \tag{28a}$$

$$\mathbf{z}_{k+1} = \mathbf{A}^d\,\mathbf{z}_k + \sum_{i=1}^{m} u_{i,k+1}\mathbf{B}_i^d\,\mathbf{z}_{k+1} + \mathcal{O}(\Delta t^2), \tag{28b}$$

where $\mathbf{A}^d = \exp(\mathbf{A}\Delta t)$, $\mathbf{B}_i^d = \mathbf{B}_i\Delta t$.

C. Least-Squares Formulation and Singular Value Truncation

Assume that the isotypic dictionary of observable functions $T(\mathbf{x}) \in \mathbb{C}^M$ is selected, we can identify the discretized KBF models (28) using least-squares formulation similar to EDMD [37], which gives us the approximated eigenfunction coordinates and the discretized KBF (28). In the following, we assume that the explicit model (28a) is used, while the implicit model (28b) can be obtained in a similar way.

Assume that the measurement data is collected from a single sampled trajectory that contains various transient responses of the DER to be modeled. Denote the state and input data point at each sampling interval as $(\mathbf{x}_k, \mathbf{u}_k)$, $k = 1, \dots, N$. In order to linearly identify (28a), the following data matrices are combined from the trajectory data as

$$\mathbf{X}_1 = \left[T(\mathbf{x}_1)\ \dots\ T(\mathbf{x}_{N-1})\right],\ \mathbf{X}_2 = \left[T(\mathbf{x}_2)\ \dots\ T(\mathbf{x}_N)\right], \tag{29}$$

and the input matrices are combined as

$$\mathbf{\Gamma}_i = \left[u_{i,1}T(\mathbf{x}_1)\ \dots\ u_{i,N-1}T(\mathbf{x}_{N-1})\right],\ i = 1, \dots, m. \tag{30}$$

Then, the approximated discrete matrices in (28a) is found by minimizing the cost function $\|\mathbf{X}_2 - \mathbf{G}\boldsymbol{\Omega}\|_F^2$ where

$$\boldsymbol{\Omega} = \begin{bmatrix} \mathbf{X}_1^\mathsf{T} & \boldsymbol{\Gamma}_1^\mathsf{T} & \dots & \boldsymbol{\Gamma}_m^\mathsf{T} \end{bmatrix}^\mathsf{T}, \tag{31}$$

and

$$\mathbf{G} = \begin{bmatrix} \mathbf{A}^d & \mathbf{B}_1^d & \dots & \mathbf{B}_m^d \end{bmatrix} \tag{32}$$

is the unknown. The least-squares problem has a closed-form solution in terms of the pseudoinverse of $\boldsymbol{\Omega}$ [47], $\widehat{\mathbf{G}} = \mathbf{X}_2\boldsymbol{\Omega}^\dagger$.

Since the assumed discretization of KBF is only first-order accurate with respect to the time step Δt and the selected observable functions are usually not guaranteed to represent the eigenspace, to regularize the solution, singular value truncation [47] needs to be applied to the solution $\widehat{\mathbf{G}}$. For the identification of discrete-time system matrices as in EDMD, singular value truncation essentially adds to the cost function a regularization term $\varepsilon\|\mathbf{G}\|_F^2$ [47].

To proceed, assume that the singular value decomposition (SVD) of $\boldsymbol{\Omega}$ is given by $\boldsymbol{\Omega} = \mathbf{U}\boldsymbol{\Sigma}\mathbf{V}^\mathsf{H}$, and the singular value truncated data matrix by $\widetilde{\boldsymbol{\Omega}} = \widetilde{\mathbf{U}}\widetilde{\boldsymbol{\Sigma}}\widetilde{\mathbf{V}}^\mathsf{H}$, where $\widetilde{\boldsymbol{\Sigma}}$ is a diagonal matrix of the reduced singular values with its dimension $R < M$. The regularized solution can then be expressed as

$$\widehat{\mathbf{G}} = \mathbf{X}_2\widetilde{\boldsymbol{\Omega}}^\dagger, \tag{33}$$

and the discrete-time system matrices are found by

$$\widehat{\mathbf{A}}^d = \mathbf{X}_2\widetilde{\mathbf{V}}\widetilde{\boldsymbol{\Sigma}}^{-1}\widetilde{\mathbf{U}}_0^\mathsf{H}, \quad \widehat{\mathbf{B}}_i^d = \mathbf{X}_2\widetilde{\mathbf{V}}\widetilde{\boldsymbol{\Sigma}}^{-1}\widetilde{\mathbf{U}}_i^\mathsf{H}, \tag{34}$$

where $\begin{bmatrix}\widetilde{\mathbf{U}}_0^\mathsf{T}, \widetilde{\mathbf{U}}_1^\mathsf{T}, \dots, \widetilde{\mathbf{U}}_m^\mathsf{T}\end{bmatrix}^\mathsf{T} = \widetilde{\mathbf{U}}$ is the appropriate partitioning of $\widetilde{\mathbf{U}}$.

The system of (34) is in the M observable coordinates, which contains the original states. The original state can be reconstructed from the predictions under certain conditions discussed in the next subsection. Now, since the rank of the system is $R < M$ by the singular value truncation, the system can be further reduced to dimension R for reduced computation in the prediction stage by taking the state transformation on the observable state $\overline{\mathbf{z}} = (\mathbf{X}_2\widetilde{\mathbf{V}})^\dagger\mathbf{z} = \mathbf{P}^\dagger\mathbf{z}$, which results in the reduced system

$$\overline{\mathbf{A}}^d = \widetilde{\boldsymbol{\Sigma}}^{-1}\widetilde{\mathbf{U}}_0^\mathsf{H}\mathbf{X}_2\widetilde{\mathbf{V}}, \quad \overline{\mathbf{B}}_i^d = \widetilde{\boldsymbol{\Sigma}}^{-1}\widetilde{\mathbf{U}}_i^\mathsf{H}\mathbf{X}_2\widetilde{\mathbf{V}}. \tag{35}$$

Here, we made the assumption that $\mathbf{X}_2\widetilde{\mathbf{V}}$ has full rank R, i.e., the least-squares problem is linearly consistent after the singular value truncation [47].

D. Original State Reconstruction

Since the isotypic functions with monomial embeddings $T(\mathbf{x})$ contains the original state vector $\mathbf{x}$, the original state can be linearly extracted from the observable state vector through a constant matrix $\mathbf{C}$ such that

$$\mathbf{x} = \mathbf{C}\mathbf{z}. \tag{36}$$

For the reduced model (35) with the reduced observable function embedding, the potential linear reconstruction takes the form

$$\mathbf{x} = \mathbf{C}\mathbf{P}\overline{\mathbf{z}} = \mathbf{C}\mathbf{P}(\mathbf{P}^\dagger\mathbf{z}). \tag{37}$$

However, due to reduction in dimension from the transformation $\overline{\mathbf{z}} = \mathbf{P}^\dagger\mathbf{z}$, the product $\mathbf{P}\mathbf{P}^\dagger$ has rank $R < M$, which means that the original state reconstruction from the reduced observable state $\overline{\mathbf{z}}$ in (37) may be ill-conditioned so that the predictions from the reconstructed state are incomplete. The prediction error resulting from original state reconstruction needs to be distinguished from the error in the Koopman approximation as the two are independent of each other. To distinguish the reconstruction error from the modeling error, in the validation step, the full embedded system (34) should be used. Then, the reduced model (35) may be used for speeding up the prediction if the original state reconstruction from the reduced observable state $\overline{\mathbf{z}}$ is well-conditioned.

IV. M-KBF Microgrid Dynamics Prediction

The prediction of the microgrid dynamics follows the usual DAE solution method of recursively advancing the KBF models (28) for the DER systems and solving the hybrid power flow equations (5). In the following, we first discuss the details of prediction of the individual KBF models of DER systems before we present the full M-KBF prediction algorithm.

Recall the isotypic observable functions and inputs derived in (18)-(22) and the real monomials for building the first part of the isotypic observable functions in (23) and (24). Because the input from the solution to the hybrid power flow is dimensional, the KBF prediction uses the the reference (V_C or $e^{j\theta}$) from the last time step to transform the input at the current time step; that is, for the GFM DER system,

$$\mathbf{z}_{k+1} = \mathbf{A}^d\mathbf{z}_k + \mathbf{B}^d\mathbf{z}_{k+1}\frac{I_N[k+1]}{V_C[k]} \tag{38}$$

with $\mathbf{x}_k = \mathbf{C}\mathbf{z}_k$, and, for the GFL DER system,

$$\mathbf{z}_{k+1} = \mathbf{A}^d\mathbf{z}_k + \mathbf{B}_1^d\mathbf{z}_{k+1}\frac{V_C[k+1]}{e^{j\theta}[k]} + \mathbf{B}_2^d\mathbf{z}_{k+1}\frac{S^{\text{ref}}[k+1]e^{j\theta}[k]}{V_C[k+1]} \tag{39}$$

with $\mathbf{x}_k = \mathbf{C}\mathbf{z}_k$.

Under perfectly identified KBF models, all elements of the observable state $\mathbf{z}_k$ of both the GFM and GFL model should always share the same complex angle, i.e., the real monomials for the first part of the observable (23) and (24) should always be real. In addition for GFL system, the first element $e^{j\theta}$ should have constant absolute value. Since the KBF model in isotypic embedding is, in theory, only valid if the observable state $\mathbf{z}_k$ is found on this manifold, small error in the KBF model, which cumulates over time to cause the observable state to leave the manifold, can lead to catastrophic failures. Thus, to make the prediction algorithm more robust to data-driven modeling errors, we add the following correction to the observable state at each time step to project the predicted state at time $k+1$ onto the manifold. For the GFM or GFL model, the corrected observable state is given by (the subscript for time is omitted),

$$\text{GFM:}\ \ \mathbf{z}^* = \text{diag}\Big\{\text{sign}\big[\text{Re}(\text{conj}(z_1)\cdot\mathbf{z})\big]\Big\}|\mathbf{z}|\frac{z_1}{|z_1|} \tag{40a}$$

$$\text{GFL:}\ \ \mathbf{z}^* = \text{diag}\Big\{\text{sign}\big[\text{Re}(\text{conj}(z_1)\cdot\mathbf{z})\big]\Big\}|\mathbf{z}|\frac{z_1}{|z_1|^2} \tag{40b}$$

where $z_1 = V_C$ for GFM or $z_1 = e^{j\theta}$ for GFL is the first observable state.

Combining the hybrid power flow equation, the data-driven KBF models in isotypic embedding for the DERs, and the manifold correction, the full M-KBF prediction algorithm for microgrid dynamics is summarized in Algorithm 1. Notice that the KBF model for both GFM and GFL DERs on Line 7 and 12 are the explicit model (28a) While in the model identification phase the implicit form (28b) is more accurate and usually gives the best results, we find in our tests that changing to the explicit form in the prediction phase produces almost identical trajectories of microgrid dynamics with reduced computation cost due to the elimination of matrix inversion.

Algorithm 1: M-KBF Enabled Prediction Algorithm

Input : KBF model for each DER system $(\mathbf{A}_p^d, \mathbf{B}_p^d, \mathbf{C}_p^d, T_p(\cdot))$, $p = 1, \ldots, |\mathcal{N}|$, hybrid network parameter matrix $\mathbf{H}$, initial conditions $\mathbf{y}^{\text{net}}[1]$, $\mathbf{u}^{\text{net}}[1]$, $\mathbf{x}_p[1]$ for $p = 1, \ldots, |\mathcal{N}|$, prediction length len, and input disturbances $\underline{S}^{\text{ld}}[k]$, $\underline{S}^{\text{ref}}[k]$ for $k = 1, \ldots, \text{len}$

Output: Predicted microgrid bus voltages and currents $\mathbf{y}^{\text{net}}[k]$, $\mathbf{u}^{\text{net}}[k]$ for $k = 1, \ldots, \text{len}$

1 $\mathbf{z}_p[1] = T_p(\mathbf{x}_p[1])$, $p = 1, \ldots, |\mathcal{N}|$;
2 **for** $k = 1$ **to** len **do**
3 Calculate DER system inputs $\underline{I}_1^{\text{gen}}$, $\underline{V}_2^{\text{gen}}$ using (6);
4 **for** $p = 1$ **to** $|\mathcal{N}|$ **do**
5 **if** Bus p is GFM **then**
6 $\mathbf{u}'_p[k+1] = \frac{I_{N,p}[k+1]}{V_{C,p}[k]}$;
7 $\hat{\mathbf{z}}_p = \big(\mathbf{A}_p^d + \sum_i \mathbf{B}_{i,p}^d u'_{i,p}[k+1]\big)\hat{\mathbf{z}}_p[k]$;
8 $\mathbf{z}_p[k+1] = \text{diag}\Big\{\text{sign}\big[\text{Re}(\text{conj}(\hat{z}_{1,p}) \cdot \hat{\mathbf{z}}_p)\big]\Big\}|\hat{\mathbf{z}}_p|\frac{\hat{z}_{1,p}}{|\hat{z}_{1,p}|}$;
9 $\mathbf{x}_p[k+1] = \mathbf{C}_p\mathbf{z}_p[k+1]$;
10 **else**
11 $\mathbf{u}'_p[k+1] = \left[\frac{V_{C,p}[k+1]}{e^{j\theta_p[k]}}, \frac{S_p^{\text{ref}}[k+1]e^{j\theta_p[k]}}{V_{C,p}[k+1]}\right]^{\mathsf{T}}$;
12 $\hat{\mathbf{z}}_p = \big(\mathbf{A}_p^d + \sum_i \mathbf{B}_{i,p}^d u'_{i,p}[k+1]\big)\hat{\mathbf{z}}_p[k]$;
13 $\mathbf{z}_p[k+1] = \text{diag}\Big\{\text{sign}\big[\text{Re}(\text{conj}(\hat{z}_{1,p}) \cdot \hat{\mathbf{z}}_p)\big]\Big\}|\hat{\mathbf{z}}_p|\frac{\hat{z}_{1,p}}{|\hat{z}_{1,p}|^2}$;
14 $\mathbf{x}_p[k+1] = \mathbf{C}_p\mathbf{z}_p[k+1]$;
15 **end if**
16 **end for**
17 Update $\underline{V}_1^{\text{gen}}[k+1]$ and $\underline{I}_2^{\text{gen}}[k+1]$;
18 Calculate hybrid power flow with input $\underline{S}^{\text{ld}}[k+1]$ based on (5) to get $\underline{I}^{\text{ld}}[k+1]$;
19 Update $\mathbf{y}^{\text{net}}[k+1]$ and $\mathbf{u}^{\text{net}}[k+1]$;
20 **end for**

V. Numerical Examples

For testing the effectiveness of M-KBF in identifying nonlinear microgrid dynamics under large disturbances, a numerical example is set up in Matlab using the microgrid system shown in Fig. 2. Details of the test system including the per-unit system, the nominal power flow condition, and the line impedance are given in the Appendix. In Fig. 2, Bus 1 is the slack bus that is connected to the grid-forming DER controlled by Vf control, and all the other DERs are grid-following generators with PQ controls. All PQ controllers have the same control parameters, which allows us to identify their KBF model built with the local data of a few PQ-controlled DERs and, in the prediction phase, apply the PQ model for all PQ-controlled DERs in the system to demonstrate the modularity of our method. All power loads in the microgrid are modeled as constant power loads. Using the DER controller model given in the Appendix, the detailed phasor model of the microgrid is built as a DAE with the approximation of quasi-static electrical network and RLC filter dynamics. Please refer to [48] for more details on the microgrid test system.

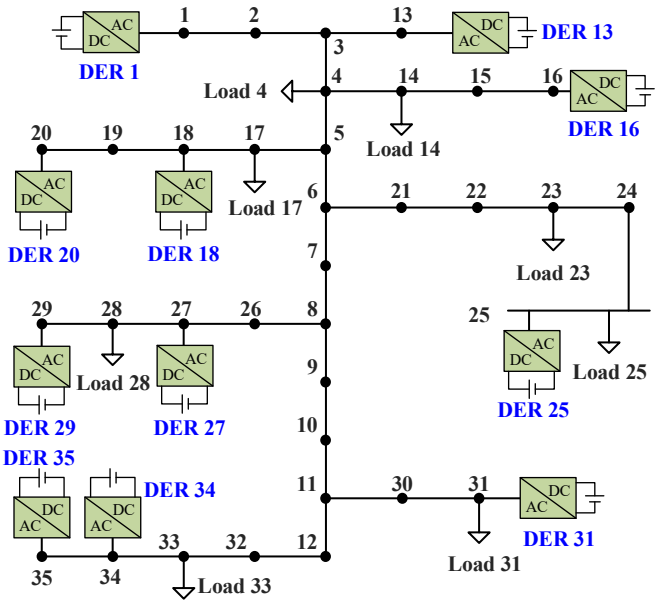

Fig. 2. Example microgrid test system

In Table 1, information about data preparation and training data size are summarized. To generate the dynamic responses of the system to provide both the training data and the test data, the DAE model is simulated with a step size of 10^{-3} s. The input to the system includes random step changes to power loads and PQ-controlled DERs' power references. Every simulated trajectory starts from the same nominal condition and spans 20 s, where random step changes of uniformly distribution are introduced to each input at every 0.5 s interval. The simulated

TABLE I
Data Preparation and Training Information

Item	Value
Simulation timescale	10^{-3} s
Koopman modeling timescale	10^{-3} s
Vf nd state/input dimension (18)	9/2
PQ nd state/input dimension (22)	8/4
Vf training data size	312 step changes (8×20 s duration)
PQ training data size	$1,248$ step changes (32×20 s duration)
Vf truncation order/# observables	100/220
PQ truncation order/# observables	70/120

This article has been accepted for publication in IEEE Transactions on Smart Grid. This is the author's version which has not been fully edited and content may change prior to final publication. Citation information: DOI 10.1109/TSG.2024.3399076

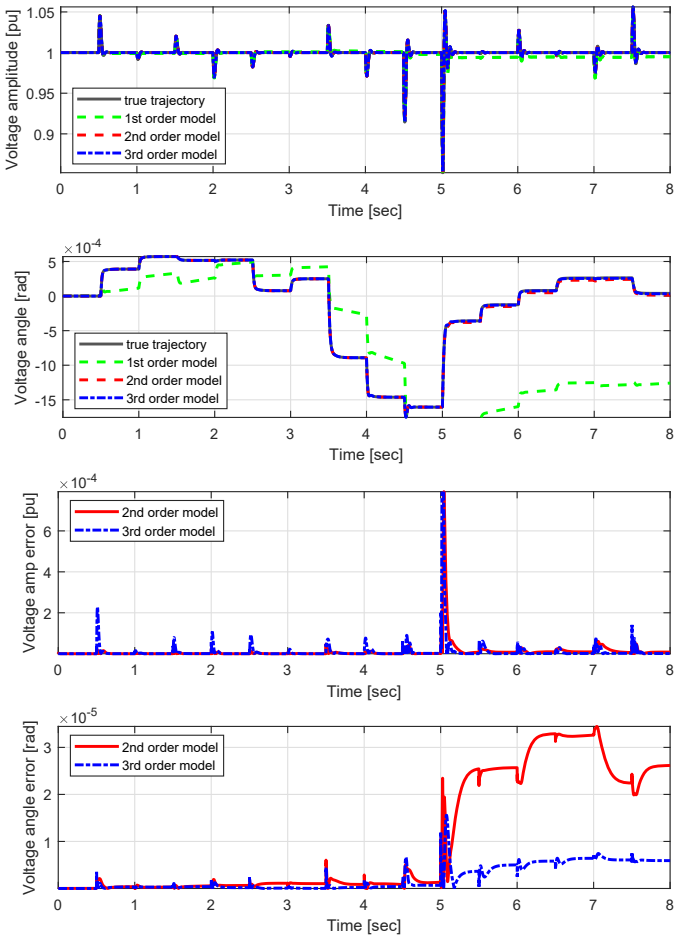

Fig. 3. Prediction and absolute errors for the Vf-controlled DER of 100%-range step changes in a 0.05 radian shifted reference frame by KBF models obtained with different orders of monomial functions

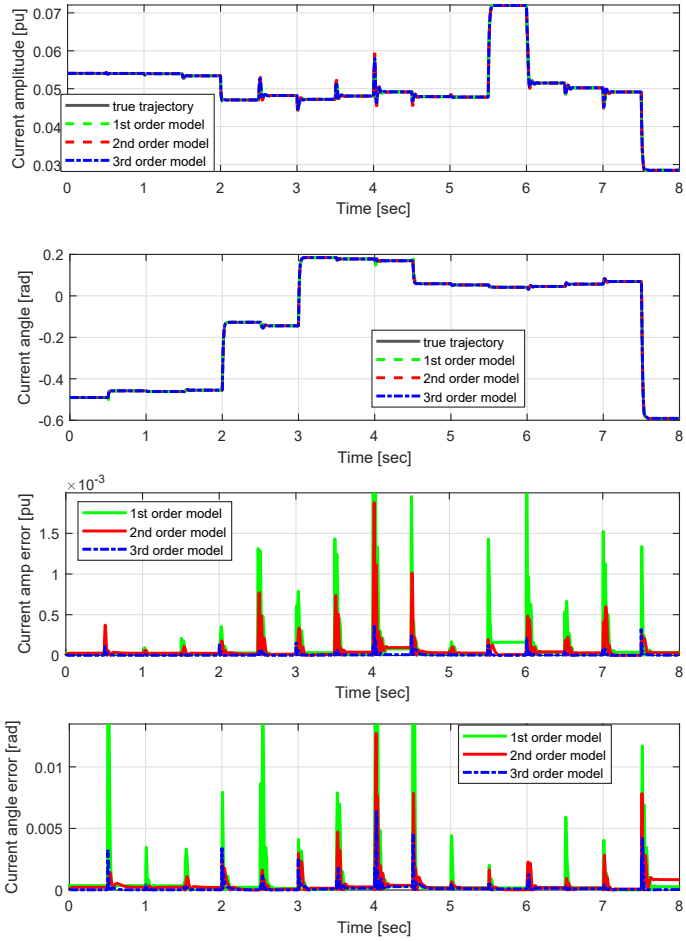

Fig. 4. Prediction and absolute errors for a PQ-controlled DER at Bus 31 of 100%-range step changes in a 0.0342 radian shifted reference frame by KBF models obtained with different orders of monomial functions

trajectories are distinguished by the percentage of the of the maximum step change magnitudes relative to the nominal conditions of each load or DER. For example, for 80% random changes, every step change has a uniform distribution in $0.8\,[-P_0,\, P_0]$ (or $0.8\,[-Q_0,\, Q_0]$) depending on the nominal power value.

A. Data-Driven Modeling for Individual DER via KBF

Thanks to the modularity of the proposed method, the DER models are trained and validated individually with only data pertaining to the DER system. The DER system interactions, in the form of transient bus current bus voltage for Vf or PQ system, serve as the perturbation for the dynamics identification without the need for separate excitation to induce larger microgrid-level transients. For the Vf system, the training data includes local data of four 20 s periods of 50% range step disturbances and four 20 s periods of 80% range step disturbances, with a total of 312 transient events. For the PQ system, the training data includes local data of the PQ DER at Bus 13, 18, and 25 during the same microgrid transients, with a total of $1,248$ transient events. Since the PQ-controlled DERs are identical, their data are combined for the training of the common KBF model. The implicit form of KBF is used for identifying both the Vf and PQ system.

The test results of the KBF models of the Vf and PQ systems are shown in Fig. 3 and Fig. 4, where the test data is part of a microgrid trajectory under 100% range step disturbances. It is worth noting the difference between the training and the prediction result in testing. Although the training data only see non-dimensional input $\mathbf{u}'$ in (19) and (22), the prediction in Fig. 3 and Fig. 4 uses the predicted reference to transform the input at each time step as in Algorithm 1. Since the input in the testing is dimensional, i.e., affected by angle symmetry, the result shows that the isotypic embedding introduced in Section III successfully separates the symmetry from the training process without the drawback of losing dynamics information in the dimensional coordinates.

Detailed explanations of the result are:

- For both the Vf model and the PQ model, an observable dictionary with up to 3rd order monomial can accurately capture the nonlinear DER dynamics. While the prediction from 2nd order model is similar, the prediction error is accumulates faster than the 3rd order model.
- For the PQ system in Fig. 4, the isotypic embedding leaves the dynamics to be learned by KBF only mildly nonlinear. While the 1st-order model can make reasonable predictions with the correction step (40b), the 3rd-order model prediction has the lowest error.

This article has been accepted for publication in IEEE Transactions on Smart Grid. This is the author's version which has not been fully edited and content may change prior to final publication. Citation information: DOI 10.1109/TSG.2024.3399076

- The nonlinearity of the Vf DER system mainly results from the complex phasor calculations and the resulting angle and amplitudes. The 1st-order model is thus not expressive enough to fit the corresponding dynamics.

B. SVD Order Truncation and Eigenfunctions

In order to obtain an appropriate KBF model for prediction and overcome the discretization error when arriving at the template model (28), it is necessary to apply singular value truncation to the data matrix. Here we show that an optimal truncation order can be inferred by the eigenvalue distribution. Fig. 5 shows the distribution of the approximated Koopman eigenvalues on the Vf model with monomial observables of up to 3rd order when different truncation orders are applied. We can see that:

- When a higher SVD truncation order (less regularization) is applied to the KBF model solution, there exists an eigenvalue pattern repetition of the eigenvalues to the right of the figure, as illustrated in Fig. 5a. This is due to the fact that the sum of two Koopman eigenvalues is another Koopman eigenvalue with the associated eigenfunction being the product of the two existing eigenfunctions, as given in (14). As a consequence, the repeated eigenvalues to the left correspond to higher order eigenfunctions that are less likely to be approximated accurately by the monomials of lower orders, which may result in an unstable KBF model for prediction.
- When the appropriate SVD truncation order is applied, the identified Koopman eigenvalues contain no repetitive pattern and the associated eigenfunctions can be well approximated by the selected low-order monomials so that the resulting KBF model is not only stable but can accurately represent the dynamics of the DER subsystem, as has been demonstrated in Fig. 3 and Fig. 4.

We have tested Vf- and PQ-controlled DER models with both the 2nd-order and 3rd-order monomials and find that in each setup there is a narrow range of SVD truncation order that results in the KBF model having the lowest prediction error. The optimal truncation order is inferred by the distribution of the identified Koopman eigenvalues by retaining only the number of eigenvalues with no repetitive pattern.

The coefficient matrices of the identified eigenfunction embeddings with the optimal SVD truncation orders for the Vf and PQ models are shown in Fig. 6 and Fig. 7, where the absolute values of the monomial coefficients of the approximated eigenfunctions are plotted. The vertical axes in both figures correspond to the eigenfunctions in the descending order of the real parts of their eigenvalues. We can see from Fig. 6 that eigenfunctions number 38 to 68, which are highlighted in Fig. 5, have large coefficients corresponding to the monomials x_3 multiplied with the first and second order combinations of the filter current, with x_3 being the state variable for the voltage amplitude outer loop. This agrees with the fact that theses variables have fast dynamics in the original DAE model.

C. Prediction Based on M-KBF and Error Analysis

Based on Algorithm 1, the independently identified KBF models are integrated to predict the whole system's transient

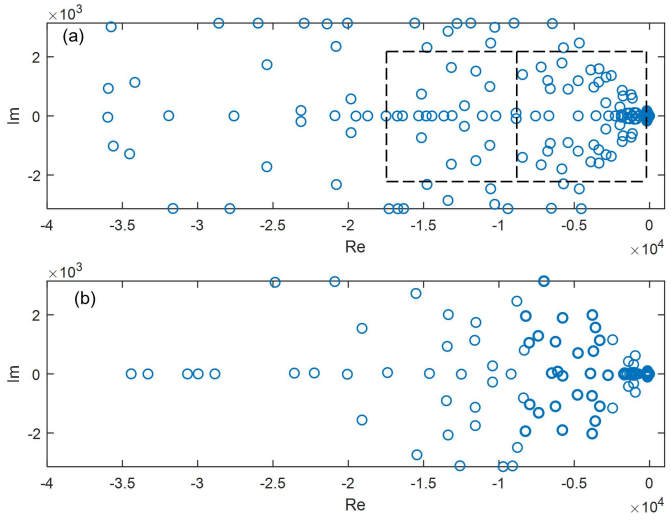

Fig. 5. The existence of repeating patterns of the locations of the transformed continuous-time eigenvalues as an indication for unusable models for prediction: (a) $r = 150$, (b) $r = 100$ (selected truncation order)

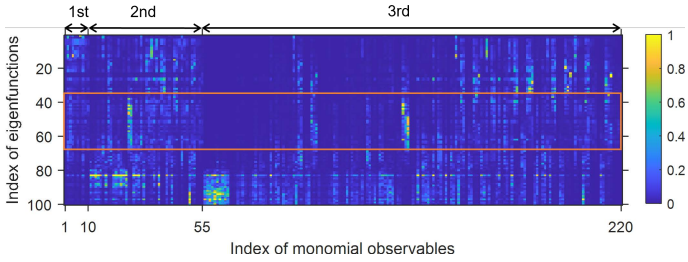

Fig. 6. Eigenfunction coefficients for Vf model

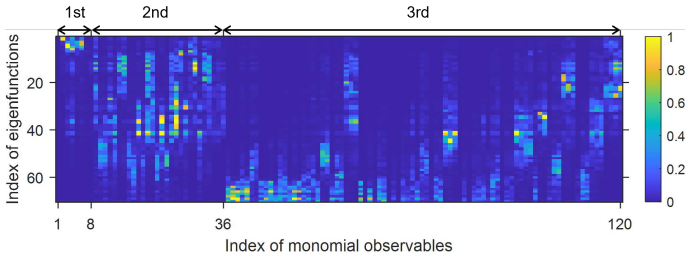

Fig. 7. Eigenfunction coefficients for PQ model

responses. Fig. 8 and Fig. 9 show the voltage and current predictions of the connected M-KBF model under 100% range disturbances. From the predictions, we can see that

- The Vf and PQ models trained on 80% range data of individual DER systems is capable of predicting 100% range disturbances of the whole microgrid system. The PQ model trained on local data of Bus 13, 18, and 25 accurately represents every PQ-controlled DER system located in different parts of the microgrid.
- The prediction results demonstrate the M-KBF's plug-and-play functionality, since the identified KBF model for PQ-controlled DERs is repeatedly used in the system.
- Every KBF model for the DER systems fully respects the angle symmetry such that the prediction of the whole system including the complex phase angle interactions is

acurately predicted without limits on the angle range of each DER.
- The prediction errors in the whole system prediction is does not accumulate as in the individual tests because each DER model's input in the connected system is a dynamic feedback from the rest of the system.

In Fig. 10, the average prediction errors are shown. For each range of disturbance, the average mean absolute percentage error (MAPE) is calculated from five test trajectories. As in Fig. 10, the bus voltage amplitude MAPEs remain below 0.01%, and the bus current MAPEs remain below 0.03% for the disturbance range of 100%. In Table II, the average simulation times for 20 s of microgrid system trajectory on a 3.6GHz PC is shown for different models and solution methods. Without the potential for parallel update of each DER model, the proposed M-KBF method uses half the time of the standard Euler method for the DAE model while being similar to the numerical differentiation formula (NDF) method.

D. Prediction under Changing Microgrid Topologies

The modularity and scalability of M-KBF is tested by prediction of the microgrid dynamics under both quadrupled and halved topology compared to the nominal 35-bus topology of Fig. 2 as well as 50% range random step disturbances. The prediction results are shown in Fig. 11. At 5.0 s, four identical microgrids with the topology in Fig. 2 are joined together, each one connected to the next one between Bus 16 and Bus 3, which results in a 140-bus connected microgrids with 44 DERs. The additional microgrid is initialized to the same state at 5.0 s as the original microgrid, and the random step changes are independent for each microgrid. At 7.5 s, the microgrid topology is halved by disconnecting the additional microgrids and, at the same time, disconnecting the part of the original microgrid below Bus 6, which results in a smaller microgrid with 19 buses and 6 DERs. The detailed discussions are:

- Since the dynamics of the microgrid consists of the interactions between the symmetry preserving KBF DER models, the prediction of M-KBF remains accurate under different system topologies and during system topology changes.
- In Fig. 11c and Fig. 11d, where the voltage amplitudes for microgrid one and four in the joined system is shown, the voltage transients are both qualitatively different than the original microgrid. This confirms the necessity of the modular design of M-KBF for reconfigurable microgrids.

Thus, the flexibility and scalability of M-KBF in terms of changing system topologies is verified.

TABLE II
SIMULATION TIMES OF 20 S TRAJECTORIES

Method	Average simulation time [s]
DAE model (Euler)	60.51
DAE model (NDF)	26.95
M-KBF	30.09

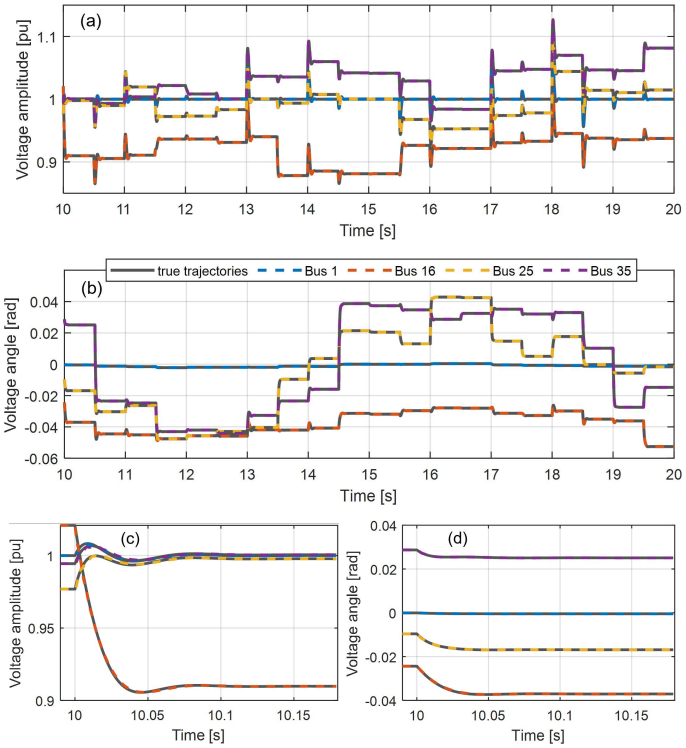

Fig. 8. Microgrid voltage dynamics prediction under 100% range random disturbances, (a) voltage amplitude, (b) voltage angle, (c) zoomed in of voltage amplitude, (d) zoomed in of voltage angle

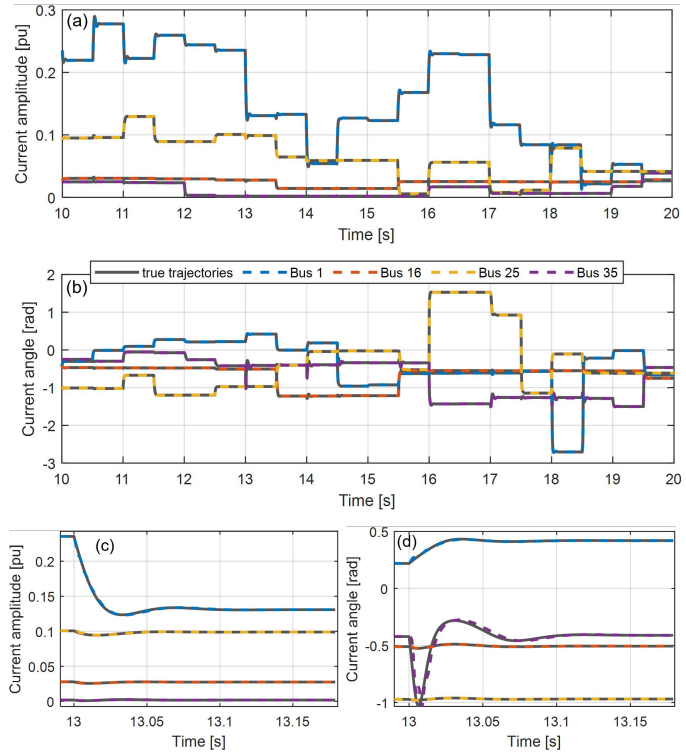

Fig. 9. Microgrid current dynamics prediction under 100% range random disturbances, (a) current amplitude, (b) current angle, (c) zoom-in of current amplitude, (d) zoom-in of current angle

VI. Conclusions and Future Work

The paper contributes a scalable data-driven method, M-KBF, to efficiently model and predict the transient dynamics

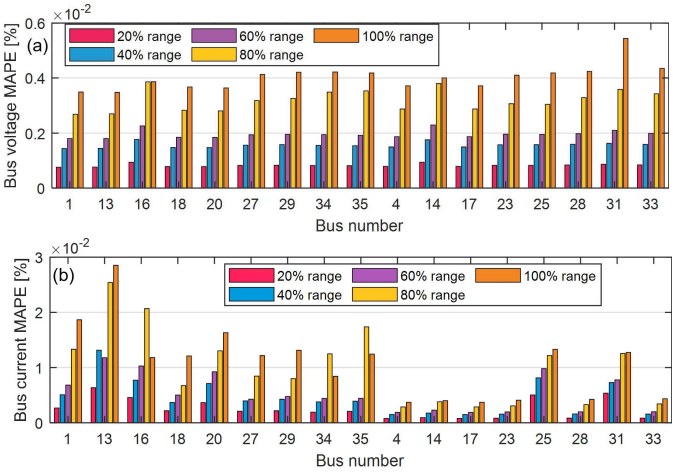

Fig. 10. Bus voltage and current prediction errors in terms of mean absolute percentage (MAPE).

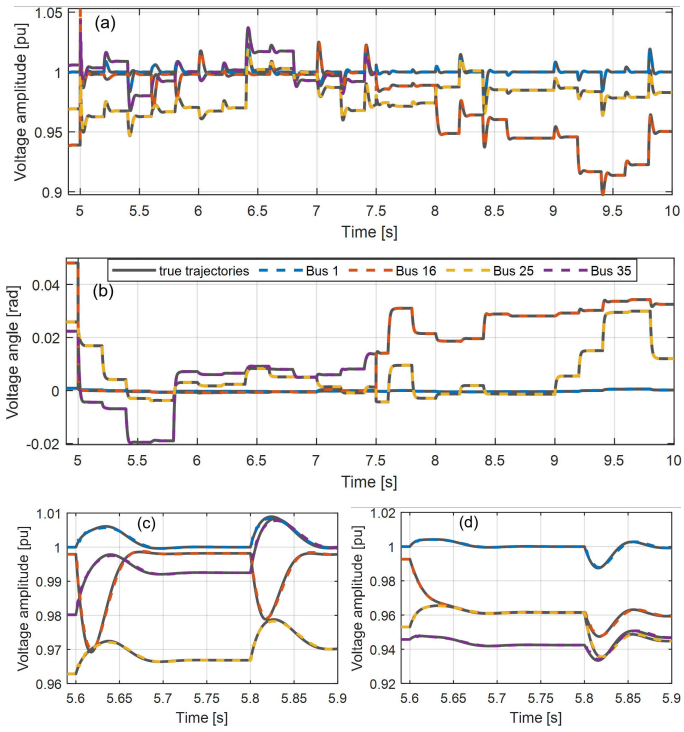

Fig. 11. Prediction under changing topology (joined by three identical microgrids between 5 and 7.5 s and isolating half of microgrid one after 7.5 s) as well as 50% range random disturbances, (a) voltage amplitude of microgrid one, (b) voltage angle of the microgrid one, (c) zoom-in of voltage amplitude of microgrid one, (d) zoom-in of voltage amplitude of microgrid four

of nonlinear microgrids under disturbances. The data-driven models for subsystems are developed through EDMD with eigenvalue-based order truncation, which are integrated into a combined model for the microgrid system. With the proposed M-KBF model, predictions of the system's responses to various external disturbances including load and generator changes and changes to the network topology can be produced in a distributed manner using the individual subsystem models. Test results have demonstrated the effectiveness of M-KBF in providing fast and precise transient predictions. For future work, M-KBF will be further developed to handle data with noise, to identify the system by using output-only measurements like bus voltage and current, and to perform predictive control based on the predictions obtained from M-KBF.

TABLE III
SYSTEM-WIDE PER-UNIT BASE

P_B	V_{Bl-l}	ω_0
1 MW	400 V	60 Hz

APPENDIX

A. Derivation of the Hybrid Parameter Matrix

Let the set of buses of the network be denoted by $\mathcal{N}$. Denote $\mathbf{Y}$ as the nodal admittance matrix, which after permutation of the rows and columns, corresponds to buses in $\mathcal{N}_1$, $\mathcal{N}_2$, and $\mathcal{N}_3$ which are respectively the GFM buses, GFL buses, and buses with no power load or generator and assumed to be mutually exclusive. Buses that are only connected to power loads is included in $\mathcal{N}_2$. Perform the following partition of $\mathbf{Y}$ according to the boundary between the buses $\mathcal{N}_1$ and $\mathcal{N}_2 \cup \mathcal{N}_3$,

$$\mathbf{Y} = \begin{bmatrix} \mathbf{Y}_{11} & \mathbf{Y}_{12} \\ \mathbf{Y}_{21} & \mathbf{Y}_{22} \end{bmatrix}. \tag{41}$$

Then, the extended hybrid parameter matrix is found as

$$\mathbf{H}' = \begin{bmatrix} \mathbf{Y}_{11} - \mathbf{Y}_{12}\mathbf{Y}_{22}^{-1}\mathbf{Y}_{21} & \mathbf{Y}_{12}\mathbf{Y}_{22}^{-1} \\ -\mathbf{Y}_{22}^{-1}\mathbf{Y}_{21} & \mathbf{Y}_{22}^{-1} \end{bmatrix}. \tag{42}$$

A sufficient condition by [41, Theorem 2] for $\mathbf{Y}_{22}$ to have full rank (invertible) is for the network to be connected and the branch resistance to be greater than zero for all branches. If this condition is satisfie, $\mathbf{H}'$ is well-defined. The hybrid parameter matrix in (1) is found by taking the upperleft square submatrix of $\mathbf{H}'$ of size $|\mathcal{N}_1| + |\mathcal{N}_2|$.

B. Phasor Model for the DER Subsystems

The DER connection circuit and the Vf-controller (given as an example) are shown in Fig. 1 and Fig. 12, respectively. Ten differential equations can then be developed, which are not given here. These equations form a control affine system, where the state vector is $\mathbf{x} = [x_1, \ldots, x_6, V_C^D, V_C^Q, I_L^D, I_L^Q]^\mathsf{T}$, the input vector is the node current $\mathbf{u} = [I_N^D, I_N^Q]^\mathsf{T}$, and the output to the network is the node voltage that is equal to the state variables $\mathbf{y} = [V_C^D, V_C^Q]^\mathsf{T}$. The input functions of the control affine system, $\mathbf{g}_1(\mathbf{x})$ and $\mathbf{g}_2(\mathbf{x})$, associated with each input are given by

$$\mathbf{g}_1(\mathbf{x}) = \left[0,\ 0,\ 0,\ 0,\ -\cos x_2,\ \sin x_2,\ \frac{1}{C},\ 0,\ -\frac{K_p^{Ireg}}{L},\ 0\right]^\mathsf{T}$$

$$\mathbf{g}_2(\mathbf{x}) = \left[0,\ 0,\ 0,\ 0,\ -\sin x_2,\ -\cos x_2,\ 0,\ \frac{1}{C},\ 0,\ -\frac{K_p^{Ireg}}{L}\right]^\mathsf{T}$$

C. Details of the Test System

The parameters of the example microgrid in Fig. 1 are given in Table III, IV, and V.

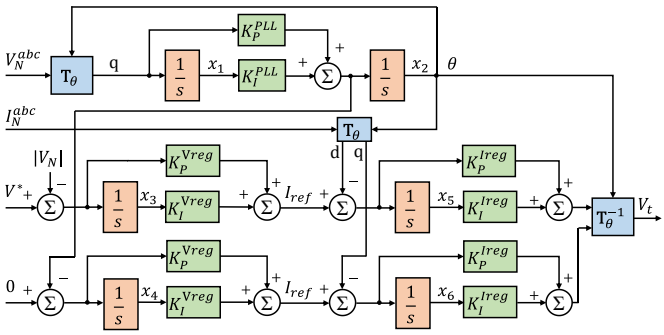

Fig. 12. Vf controller with the phase-locked loop (PLL)

TABLE IV
NOMINAL POWER FLOW CONDITION [kW]

DERs			Loads		
Bus	P_0	Q_0	**Bus**	P_0	Q_0
1	190.93	102.96	**4**	-32.69	-15.97
13	5.36	3.65	**14**	-74.69	-41.26
16	15.36	10.25	**17**	-41.56	-27.64
18	20.00	15.25	**23**	-59.63	-38.57
20	10.25	5.68	**25**	-60.54	-40.63
25	64.59	54.26	**28**	-61.35	-37.59
27	25.69	15.75	**31**	-58.21	-36.78
29	25.00	12.00	**33**	-65.31	-39.45
31	45.30	30.65			
34	36.78	14.23			
35	29.24	14.96			

TABLE V
LINE IMPEDANCE

From	To	Impedance [pu]	From	To	Impedance [pu]
3	**4**	0.0763 + j 0.0197	**21**	**22**	0.0986 + j 0.0214
5	**6**	0.0763 + j 0.0197	**22**	**23**	0.0986 + j 0.0214
7	**8**	0.0763 + j 0.0197	**23**	**24**	0.0986 + j 0.0214
9	**10**	0.0763 + j 0.0197	**24**	**25**	0.0986 + j 0.0214
10	**11**	0.0763 + j 0.0197	**26**	**27**	0.1962 + j 0.0180
11	**12**	0.0763 + j 0.0197	**27**	**28**	0.1962 + j 0.0180
3	**13**	0.9750 + j 0.0272	**28**	**29**	0.1962 + j 0.0180
4	**14**	0.9750 + j 0.0272	**30**	**31**	0.8550 + j 0.0214
14	**15**	0.9750 + j 0.0272	**32**	**33**	0.2365 + j 0.0138
15	**16**	0.9750 + j 0.0272	**33**	**34**	0.2365 + j 0.0138
17	**18**	0.3074 + j 0.0153	**34**	**35**	0.2365 + j 0.0138
18	**19**	0.3074 + j 0.0153			
19	**20**	0.3074 + j 0.0153			

REFERENCES

[1] J. Hauer, "Application of prony analysis to the determination of modal content and equivalent models for measured power system response," *IEEE Transactions on Power Systems*, vol. 6, no. 3, pp. 1062–1068, 1991.

[2] D. J. Trudnowski and J. W. Pierre, "Overview of algorithms for estimating swing modes from measured responses," in *2009 IEEE Power Energy Society General Meeting*, 2009, pp. 1–8.

[3] I. Kamwa, R. Grondin, E. Dickinson, and S. Fortin, "A minimal realization approach to reduced-order modelling and modal analysis for power system response signals," *IEEE Transactions on Power Systems*, vol. 8, no. 3, pp. 1020–1029, 1993.

[4] J. Sanchez-Gasca and J. Chow, "Performance comparison of three identification methods for the analysis of electromechanical oscillations," *IEEE Transactions on Power Systems*, vol. 14, no. 3, pp. 995–1002, 1999.

[5] L. L. Grant and M. L. Crow, "Comparison of matrix pencil and prony methods for power system modal analysis of noisy signals," in *2011 North American Power Symposium*, 2011, pp. 1–7.

[6] G. Liu, J. Quintero, and V. M. Venkatasubramanian, "Oscillation monitoring system based on wide area synchrophasors in power systems," in *2007 iREP Symposium - Bulk Power System Dynamics and Control - VII. Revitalizing Operational Reliability*, 2007, pp. 1–13.

[7] A. F. El Hamalawy, M. Ammar, H. F. Sindi, M. F. Shaaban, and H. H. Zeineldin, "A subspace identification technique for real time stability assessment of droop based microgrids," *IEEE Transactions on Power Systems*, pp. 1–1, 2021.

[8] M. G. Anderson, N. Zhou, J. W. Pierre, and R. W. Wies, "Bootstrap-based confidence interval estimates for electromechanical modes from multiple output analysis of measured ambient data," *IEEE Transactions on Power Systems*, vol. 20, no. 2, pp. 943–950, 2005.

[9] G. Liu and V. Venkatasubramanian, "Oscillation monitoring from ambient pmu measurements by frequency domain decomposition," in *2008 IEEE International Symposium on Circuits and Systems*. IEEE, 2008, pp. 2821–2824.

[10] P. Stoica, R. L. Moses *et al.*, *Spectral analysis of signals*. Pearson Prentice Hall Upper Saddle River, NJ, 2005.

[11] H. N. Villegas Pico, B. Mather, and G.-S. Seo, "Model identification of inverter nonlinear control dynamics," in *2018 IEEE Electronic Power Grid (eGrid)*, 2018, pp. 1–6.

[12] R. Fard, M. Karrari, and O. Malik, "Synchronous generator model identification for control application using volterra series," *IEEE Transactions on Energy Conversion*, vol. 20, no. 4, pp. 852–858, 2005.

[13] S. L. Brunton, J. L. Proctor, and J. N. Kutz, "Discovering governing equations from data by sparse identification of nonlinear dynamical systems," *Proceedings of the national academy of sciences*, vol. 113, no. 15, pp. 3932–3937, 2016.

[14] A. Alzahrani, M. Ferdowsi, P. Shamsi, and C. H. Dagli, "Modeling and simulation of microgrid," *Procedia Computer Science*, vol. 114, pp. 392–400, 2017.

[15] K. Emami, T. Fernando, H. H.-C. Iu, H. Trinh, and K. P. Wong, "Particle filter approach to dynamic state estimation of generators in power systems," *IEEE transactions on power systems*, vol. 30, no. 5, pp. 2665–2675, 2014.

[16] J. Qi, J. Wang, and K. Sun, "Efficient estimation of component interactions for cascading failure analysis by em algorithm," *IEEE Transactions on Power Systems*, vol. 33, no. 3, pp. 3153–3161, 2017.

[17] I. Mezić, "Spectral properties of dynamical systems, model reduction and decompositions," *Nonlinear Dynamics*, vol. 41, no. 1, pp. 309–325, 2005.

[18] I. Mezić and A. Banaszuk, "Comparison of systems with complex behavior," *Physica D: Nonlinear Phenomena*, vol. 197, no. 1-2, pp. 101–133, 2004.

[19] I. Mezic, "Koopman operator, geometry, and learning of dynamical systems," *Notices of the AMS*, vol. 68, no. 7, pp. 1087–1105, 2021.

[20] M. Budišić, R. Mohr, and I. Mezić, "Applied Koopmanism," *Chaos: An Interdisciplinary Journal of Nonlinear Science*, vol. 22, no. 4, 2012.

[21] M. Netto, Y. Susuki, V. Krishnan, and Y. Zhang, "On analytical construction of observable functions in extended dynamic mode decomposition for nonlinear estimation and prediction," in *2021 American Control Conference (ACC)*. IEEE, 2021, pp. 4190–4195.

[22] G. Mamakoukas, M. L. Castano, X. Tan, and T. D. Murphey, "Derivative-based Koopman operators for real-time control of robotic systems," *IEEE Transactions on Robotics*, vol. 37, no. 6, pp. 2173–2192, 2021.

[23] Z. Ma, Z. Wang, and R. Cheng, "Analytical large-signal modeling of inverter-based microgrids with Koopman operator theory for autonomous control," *IEEE Transactions on Smart Grid*, 2023.

[24] I. Mezić, "Analysis of fluid flows via spectral properties of the Koopman operator," *Annual Review of Fluid Mechanics*, vol. 45, pp. 357–378, 2013.

[25] M. O. Williams, I. G. Kevrekidis, and C. W. Rowley, "A data–driven approximation of the Koopman operator: Extending dynamic mode decomposition," *Journal of Nonlinear Science*, vol. 25, no. 6, pp. 1307–1346, 2015.

[26] M. O. Williams, C. W. Rowley, and I. G. Kevrekidis, "A kernel-based method for data-driven Koopman spectral analysis," *Journal of Computational Dynamics*, vol. 2, no. 2, p. 247, 2015.

[27] P. Sharma, V. Ajjarapu, and U. Vaidya, "Data-driven identification of nonlinear power system dynamics using output-only measurements," *IEEE Transactions on Power Systems*, 2021.

[28] H. Arbabi and I. Mezic, "Ergodic theory, dynamic mode decomposition, and computation of spectral properties of the Koopman operator," *SIAM Journal on Applied Dynamical Systems*, vol. 16, no. 4, pp. 2096–2126, 2017.

[29] C. Folkestad, D. Pastor, I. Mezic, R. Mohr, M. Fonoberova, and J. Burdick, "Extended dynamic mode decomposition with learned Koopman

eigenfunctions for prediction and control," in *2020 american control conference (acc)*. IEEE, 2020, pp. 3906–3913.
[30] M. Korda and I. Mezić, "Optimal construction of Koopman eigenfunctions for prediction and control," *IEEE Transactions on Automatic Control*, vol. 65, no. 12, pp. 5114–5129, 2020.
[31] Y. Susuki and I. Mezić, "Nonlinear Koopman modes and power system stability assessment without models," *IEEE Transactions on Power Systems*, vol. 29, no. 2, pp. 899–907, 2013.
[32] M. Korda, Y. Susuki, and I. Mezić, "Power grid transient stabilization using Koopman model predictive control," *IFAC-PapersOnLine*, vol. 51, no. 28, pp. 297–302, 2018.
[33] X. Li, C. Mishra, S. Chen, Y. Wang, and J. De La Ree, "Determination of parameters of time-delayed embedding algorithm using Koopman operator-based model predictive frequency control," *CSEE Journal of Power and Energy Systems*, vol. 7, no. 6, pp. 1140–1151, 2021.
[34] X. Gong and X. Wang, "A novel Koopman-inspired method for the secondary control of microgrids with grid-forming and grid-following sources," *Applied Energy*, vol. 333, p. 120631, 2023.
[35] X. Gong, X. Wang, and G. Joos, "An online data-driven method for microgrid secondary voltage and frequency control with ensemble Koopman modeling," *IEEE Transactions on Smart Grid*, vol. 14, no. 1, pp. 68–81, 2022.
[36] M. H. Roos, P. H. Nguyen, J. Morren, and J. Slootweg, "Aggregation of component-based grid-feeding der and load models for simulation of microgrid islanding transients," *Electric Power Systems Research*, vol. 189, p. 106759, 2020.
[37] J. L. Proctor, S. L. Brunton, and J. N. Kutz, "Dynamic mode decomposition with control," *SIAM Journal on Applied Dynamical Systems*, vol. 15, no. 1, pp. 142–161, 2016.
[38] F. Cecati, R. Zhu, M. Liserre, and X. Wang, "Nonlinear modular state-space modeling of power-electronics-based power systems," *IEEE Transactions on Power Electronics*, vol. 37, no. 5, pp. 6102–6115, 2021.
[39] A. Surana, "Koopman operator based observer synthesis for control-affine nonlinear systems," in *2016 IEEE 55th Conference on Decision and Control (CDC)*. IEEE, 2016, pp. 6492–6499.
[40] D. Goswami and D. A. Paley, "Bilinearization, reachability, and optimal control of control-affine nonlinear systems: A Koopman spectral approach," *IEEE Transactions on Automatic Control*, 2021.
[41] A. M. Kettner and M. Paolone, "On the properties of the power systems nodal admittance matrix," *IEEE Transactions on Power Systems*, vol. 33, no. 1, pp. 1130–1131, 2017.
[42] M. Farrokhabadi, C. A. Canizares, J. W. Simpson-Porco, E. Nasr, L. Fan, P. A. Mendoza-Araya, R. Tonkoski, U. Tamrakar, N. Hatziargyriou, D. Lagos *et al.*, "Microgrid stability definitions, analysis, and examples," *IEEE Transactions on Power Systems*, vol. 35, no. 1, pp. 13–29, 2019.
[43] A. M. Kettner, L. Reyes-Chamorro, J. K. M. Becker, Z. Zou, M. Liserre, and M. Paolone, "Harmonic power-flow study of polyphase grids with converter-interfaced distributed energy resources—part i: Modeling framework and algorithm," *IEEE Transactions on Smart Grid*, vol. 13, no. 1, pp. 458–469, 2021.
[44] A. Mauroy and I. Mezić, "Global stability analysis using the eigenfunctions of the Koopman operator," *IEEE Transactions on Automatic Control*, vol. 61, no. 11, pp. 3356–3369, 2016.
[45] A. Salova, J. Emenheiser, A. Rupe, J. P. Crutchfield, and R. M. D'Souza, "Koopman operator and its approximations for systems with symmetries," *Chaos: An Interdisciplinary Journal of Nonlinear Science*, vol. 29, no. 9, p. 093128, 2019.
[46] A. L. Bruce, V. M. Zeidan, and D. S. Bernstein, "What is the Koopman operator? a simplified treatment for discrete-time systems," in *2019 American Control Conference (ACC)*. IEEE, 2019, pp. 1912–1917.
[47] C. L. Lawson and R. J. Hanson, *Solving least squares problems*. SIAM, 1995.
[48] Y. Li, *Cyber-Physical Microgrids*. Springer, 2021.

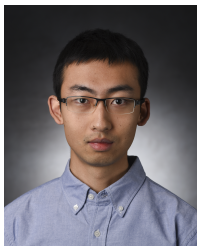

Xinyuan Jiang (Graduate Student Member, IEEE) received the B.S. degrees in electrical engineering from the North China Electric Power University, Baoding, China, and Illinois Institute of Technology, Chicago, IL, USA, both in 2017. He is currently working toward his Ph.D. degree in electrical engineering at the Pennsylvania State University, University Park, PA, USA. His research interests focus on Koopman operator, port-Hamiltonian system, and symmetry related methods in analyzing and designing distributed control in microgrids.

Yan Li (Senior Member, IEEE) received the B.Sc. and Ph.D. degrees in electrical engineering from Tianjin University, Tianjin, China, in 2008 and 2013, respectively, and her second Ph.D. degree in electrical engineering from the University of Connecticut, Storrs, CT, USA, in 2019. She joined the Electrical Engineering Department of Pennsylvania State University, University Park, PA, USA, as an Assistant Professor in August 2019. Her research interests include data-driven modeling and control, quantum computing, renewable energy and microgrids, power system stability, software-defined networking, and cyber-physical security.

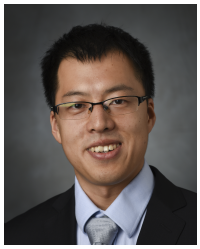

Daning Huang received the Ph.D. degree in aerospace engineering from the University of Michigan in 2019, following which he joined the Pennsylvania State University as an Assistant Professor in aerospace engineering. His current research interests include multi-disciplinary system analysis and optimization, as well as modeling and control of high-dimensional dynamical systems on complex topology.